ORIGINAL ARTICLE

A Comparison of Deep Learning and Pharmacokinetic Model Selection Methods in Segmentation of High-Grade Glioma

Azimeh NV Dehkordi [1*], Sedigheh Sina [2,3], Freshteh Khodadadi [2]

[1] *Department of Physics, Najafabad Branch, Islamic Azad University, Najafabad, Iran*

[2] *Department of Mechanic, Shiraz University, Shiraz, Iran*

[3] *Radiation Research Center, Shiraz University, Shiraz, Iran*

*Corresponding Author: Azimeh NV Dehkordi
Email: noorizadeh.az@gmail.com

Received: 18 November 2020 / Accepted: 31 December 2020

Abstract

Purpose: Glioma tumor segmentation is an essential step in clinical decision making. Recently, computer-aided methods have been widely used for rapid and accurate delineation of the tumor regions. Methods based on image feature extraction can be used as fast methods, while segmentation based on the physiology and pharmacokinetic of the tissues is more accurate. This study aims to compare the performance of tumor segmentation based on these two different methods.

Materials and Methods: Nested Model Selection (NMS) based on Extended-Toft's model was applied to 190 Dynamic Contrast-Enhanced MRI (DCE-MRI) slices acquired from 25 Glioblastoma Multiforme (GBM) patients in 70 time-points. A model with three pharmacokinetic parameters, Model 3, is usually assigned to tumor voxel based on the time-contrast concentration signal. We utilized Deep-Net as a CNN network, based on Deeplabv3+ and layers of pre-trained resnet18, which has been trained with 17288 T1-Contrast MRI slices with HGG brain tumor to predict the tumor region in our 190 DCE MRI T1 images. The NMS-based physiological tumor segmentation was considered as a reference to compare the results of tumor segmentation by Deep-Net. Dice, Jaccard, and overlay similarity coefficients were used to evaluate the tumor segmentation accuracy and reliability of the Deep tumor segmentation method.

Results: The results showed a relatively high similarity coefficient (Dice coefficient: 0.73±0.15, Jaccard coefficient: 0.66±0.17, and overlay coefficient: 0.71±0.15) between deep learning tumor segmentation and the tumor region identified by the NMS method. The results indicate that the deep learning methods may be used as accurate and robust tumor segmentation.

Conclusion: Deep learning-based segmentation can play a significant role to increase the segmentation accuracy in clinical application, if their training process is completely automatic and independent from human error.

Keywords: Pharmacokinetic Analysis; Nested Model Selection; T1-Weighted Contrast Enhanced Magnetic Resonance Imaging; Tumor Segmentation; Deep Learning-Based Algorithm.

DOI: https://doi.org/10.18502/fbt.v8i1.5858

Frontiers in BIOMEDICAL TECHNOLOGIES

1. Introduction

Tumor segmentation is an important and fundamental step in assessing the brain tumor situation and planning for an appropriate treatment approach. Measurement of tumor parameters after each treatment to assess the tumor response needs an accurate voxel-wise segmentation of the tumor region [1]. Manual tumor delineation is a time-consuming process that requires a group of clinical experts. Therefore, it can be easily affected by human error. Many researchers have focused on computer-aided techniques such as image processing [2, 3], artificial intelligence [4], fuzzy clustering methods [5, 6], and more recently, deep alignment algorithms [7-11] to increase the accuracy and speed of the tumor segmentation process. Recently, machine learning-based methods have been successfully used in clinical applications and played a significant role in increasing accuracy and speed for diagnosis and treatment of diseases, including brain tumors. In the meantime, a major part of machine learning applications has been used in the field of tumor segmentation. In the last decade, the tumor segmentation based on deep neural networks achieved the state-of-the-art performance in clinical image recognition and segmentation. Deep neural networks have been widely used for tumor segmentation in the last few years. Deep learning-based methods have been presented as reasonable and accurate tumor segmentation method in the recent investigations [12-17]. Convolutional neural networks, CNNs, are capable of learning the most useful image features automatically. It is necessary to mention that neither manual segmentation nor feature selection are required by the aforementioned networks, thus they have been extensively used in tumor segmentation [18]. The previous reports implied a successful experience of employing the deep convolutional network in the segmentation tasks [8, 12, 19, 20]. Most of the previously trained deep neural networks were assessed against the manually drawn region of interest by one or a group of experienced radiologists. The different convolutional network structure such as U-Net [12-14, 21], Dilated Residual Network (DRN) [22], Deeplabv3+ based on Xception layers [23] was employed to determine the tumor region. Their results indicated a reasonable and acceptable agreement of the deep learning-based method and manual methods. The reported Dice similarity coefficient for brain enhanced tumor segmentation was mostly between 0.57 to 0.8 [22, 24-28]. A few developed deep convolutional neural networks showed a Dice similarity coefficient greater than 0.8 [20, 29, 30]. For example, Zeineldin *et al.* [31] showed that U-Net architecture can be utilized for the segmentation of the tumor from Flair MR images with dice similarity index of 0.81 to 0.84. Havaei *et al.* [11] combined local and global 2D features extracted by a CNN for brain tumor segmentation. Kamnitsas *et al.* [32] used a 3D CNN to exploit multi-scale volumetric features which resulted in better segmentation performance than 2D CNNs. Isensee *et al.* [14] applied 3D U-Net in brain tumor segmentation with a carefully designed training process. An indispensable point is that voxel-wise class labels, determined by expert radiologists, are needed for training all deep learning algorithms which completely depends on the experience and accuracy of the expert radiologists, and is subject to human error. While physiological-based segmentation methods are more accurate and reliable for distinguishing the tumor region from the normal tissue without the need of any human interference. Indeed, angiogenesis and diffusion of contrast agent from intravascular to interstitial space in the tumor region are different from normal tissues. Therefore, there are some differences between the pharmacokinetic descriptive models of tumors and the normal tissues, and this point may be an effective method to determine the tumor extent. T1-weighted Dynamic Contrast-Enhanced MRI (DCE-MRI) provides the time information of contrast agent concentration and its distribution through the tissues [33]. DCE-MRI data analysis associated with the Nested Model Selection (NMS) concept [34] allows a reliable selection of the model and model parameters best fitted to the data. The NMS technique considers three different models with one, two, or three parameters extracted from the standard Toft's equation [33] to describe the different pharmacokinetic conditions of enhancing tumor and normal tissues in brain studies. The brain tumor progression is accompanied by the formation of new blood vessels that are structurally and functionally abnormal with disrupted Blood-Brain Barrier (BBB) [35]. Therefore, the attributed pharmacokinetic model of the tumor region in the NMS technique would be completely different from normal tissues [34-37]. It is expected that the physiological tumor segmentation would be more precise than the methods only based on the image features, thus the automated tumor segmentation method may be a straightforward and reliable approach for clinical applications, if it adapts with physiologic segmentation. In

this study, the accuracy and precision of a trained deep convolution neural network have been investigated in comparison with the physiological segmentation of tumors based on the extended Toft's model and the NMS technique.

2. Materials and Methods

2.1. Patient Data

190 DCE-MRI Slices (256×256) from 25 Glioblastoma Multiforme (GBM, High-Grade Glioma brain tumor type) patients were used in this study. The images were acquired before performing any treatment on these patients (treatment naïve patients). All available slices with an observable tumor were included in the study. A 3-T MR system was used to acquire DCE-T1 studies of all patients. Prior to the administration of contrast agent (CA, Magnevist), a driven equilibrium single pulse observation of T1 with variable flip angle (θ of 2°, 5°, 10°, 15°, 20°, and 25°) was acquired to determine the pre-contrast T1. A three-dimensional DCE-T1 Spoiled Gradient Recalled Echo (SPGR) sequence was performed using the following parameters: 70 image phases; a temporal resolution of 5.035 s; flip angle of 20°; TE/TR ~ 0.84/5.8 ms; matrix of 256 × 256; the field of view of 240 mm^2.

2.2. Nested Model Selection and Tumor Region

The Toft's model is very popular in the pharmacokinetic analysis of DCE-MRI data. The extended Toft's model describes the distribution of the contrast agent from the blood plasma into interstitial space (Equation 1). The parameters of the Toft's equation are blood plasma which is known as v_p, the forward transfer constant as K_{trans}, and inverse transfer constant as k_{ep} [33],

$$C_t(t) = K^{trans} \int_0^t e^{-k_{ep}(t-\tau)} C_p(\tau)\, d\tau + v_p C_p(t) \quad (1)$$

Where C_t is tissue contrast agent concentration and Cp is contrast concentration in blood plasma which is known as Arterial Input Function (AIF). In different pathologies such as normal or tumor tissue, the special status of the Toft's equation can be observed as a Nested Model Selection (NMS) concept [34]. The NMS concept considers three distinct physiology conditions for different brain tissue pathologies and consequently extracts three different nested models from Toft's equation to describe their pharmacokinetic. First Model of the NMS, Model 1, has one parameter which refers to normal brain tissues, where there is no detectable microvascular leakage of Contrast Agent (CA); Second Model of the NMS, Model 2, possesses two parameters which define pathologies that the CA leaks from the microvasculature; and third model of the NMS, Model 3, with three parameters fits pathologies having enough efflux of CA from intravascular space to interstitial space and then the CA re-enters the microvasculature from the interstitial space [34, 36]. Table 1 tabulates the aforementioned nested models and their parameters [23, 25, 26, 34]. The voxels located in the tumor area have enough leakage into the interstitial space due to severe BBB damage and then CA is allowed to return into the blood plasma. Therefore, the most suitable model for the fit to the dynamic time signal of tumor voxels is Model 3 of NMS.

Pharmacokinetic analysis was performed on all voxels of 190 studied slices using Maximum Likelihood Estimator (MLE) and then the goodness of fit for every two competing models was assessed voxel-wised using

Table 1. The number of parameters, symbol of each parameter, and the describing equation for three nested models [20, 22]

NMS	Name of parameters	Symbol of parameter	Equation
Model 1	Blood Plasma	v_p	$C_t(t) = v_p C_p(t)$
Model 2	Blood Plasma Forward Transfer Constant	v_p K^{trans}	$C_t(t) = K^{trans} \int_0^t C_p(\tau)d\tau + v_p C_p(t)$
Model 3	Blood Plasma Forward Transfer Constant Inverse Transfer Constant	v_p K^{trans} k_{ep}	$C_t(t) = K^{trans} \int_0^t e^{-k_{ep}(t-\tau)} C_p(\tau)d\tau + v_p C_p(t)$

Likelihood Ratio Test (LRT) with Confidence Level of 95%, and Degree of Freedom of 1 [15, 37, 38]. A normalized population-averaged Arterial Input Function (AIF) was used in the pharmacokinetic analysis.

2.3. Deep Learning-Based Segmentation

A trained Deep segmentation network (Deep-Net) based on Deeplabv3+ architecture using the weights of resnet18 pre-train Convolutional Neural Networks (CNN) was used to segment the tumor region for 190 studied slices. The deep network was trained by 17288 T1 weighted MR slices with Gadolinium-based contrast agents (T1-ce) of 293 high-grade glioma patients. The used dataset for training the Deep-Net was taken from the BraTS2020 dataset [17]. Manual segmentation of enhanced tumor, edema, and necrotic area, performed by a group of experienced radiologists (11 radiologists) was used in the training process [17]. Since the data of 190 slices used in this study was dynamic, and CA concentration was measured in 70 temporal points for each slice, the 35th time point was chosen to be used as test data for the trained Deep-Net. The data was also normalized, resized and their contrast was adjusted to be appropriate as input for the deep CNN algorithm.

2.4. Accuracy and Precision Evaluation

To evaluate the similarity of the Deep learning-based tumor segmentation with the physiological tumor segmentation, similarity indexes such as the Sørensen index (Dice similarity coefficient, DSC) [39, 40], Jaccard Similarity Coefficient (JSC) [41], and Over Lap Coefficient (OLC) [42] were applied.

2.4.1. Dice Coefficient

The Sørensen index or, in other words, Dice Similarity Coefficient (DSC), [39, 40], which equals twice the number of voxels common in segmented regions by the Deep-Net, SEG_{Deep}, and by the Nested Model Selection, i.e. SEG_{NMS}, for tumor divided by the sum of the number of voxels in each segmented area, was calculated for all 190 studied slices (Equation 2).

$$DSC = \frac{2(SEG_{Deep} \cap SEG_{NMS})}{SEG_{Deep} \cup SEG_{NMS}} \quad (2)$$

2.4.2. Jaccard Index

The Jaccard Index [41], known as the Jaccard Similarity Coefficient (JSC), was also used in evaluating the similarities between the two segmented regions. The measurement emphasizes the similarity among finite sample sets and is formally defined as the size of the intersection divided by the size of the union of the segmented regions by each method (Equation 3).

$$JSC = \frac{SEG_{Deep} \cap SEG_{NMS}}{SEG_{Deep} \cup SEG_{NMS}} \quad (3)$$

2.4.3. Overlap Coefficient

Overlap Coefficient [42] measures the similarity between two tumor segmented regions like the Jaccard index. It is defined as the intersection between two segmented areas divided by the smaller size of the two regions (Equation 4).

$$OLC = \frac{SEG_{Deep} \cap SEG_{NMS}}{\min(SEG_{Deep}.SEG_{NMS})} \quad (4)$$

3. Results

3.1. NMS Segmentation Results

The nested model selection technique based on extended Toft's equation was applied to all 190 DCE-MRI slices of 25 GBM patients. The measured time-contrast concentration of each voxel is a function of its pharmacokinetic condition in DCE-MRI studies. The NMS technique assigns a Model to each voxel, based on the various pharmacokinetic conditions and different time-contrast concentration curves between the tumor and surrounding tissues. Figure 1 determines three examples of the experimental time-concentration of CA

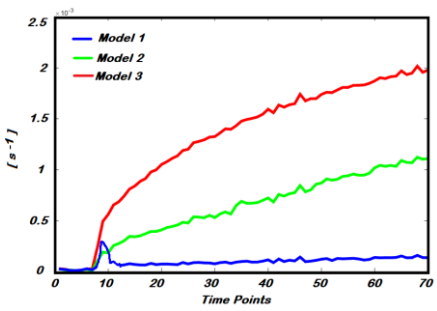

Figure 1. Three samples experimental time- CA concentration curves for Model 1 (Blue curve), Model 2 (Green curve), and Model 3 (Red curve)

curves for Model 1 (blue curve), Model 2 (green curve), and Model 3 (red curve).

Figure 2 demonstrates three sample slices of NMS brain maps generated for the three slices. In this figure, the first column shows the 35th time point of the DCE-MR images of three slices from three different patients and the second column shows their corresponding generated NMS maps. In the NMS maps, the blue, green, and red colors are attributed to the first, second, and third models, respectively. As seen in this figure, the tumor region was specified by Model 3 (red color).

However, the voxels on the major vessels were also identified as Model 3, this is acceptable since in major vessels the forward and backward transfer constants of CA are occurred through the blood plasma and could be considered equal. Figure 2 exhibits that the NMS technique can successfully outstand the tumor area from surrounding tissues by assigning the different Models to various pathologies. The voxels in the tumor area specified as Model 3 refer to the enhanced tumor which is separated from the necrotic area in the core of the tumor and edema around the enhanced tumor.

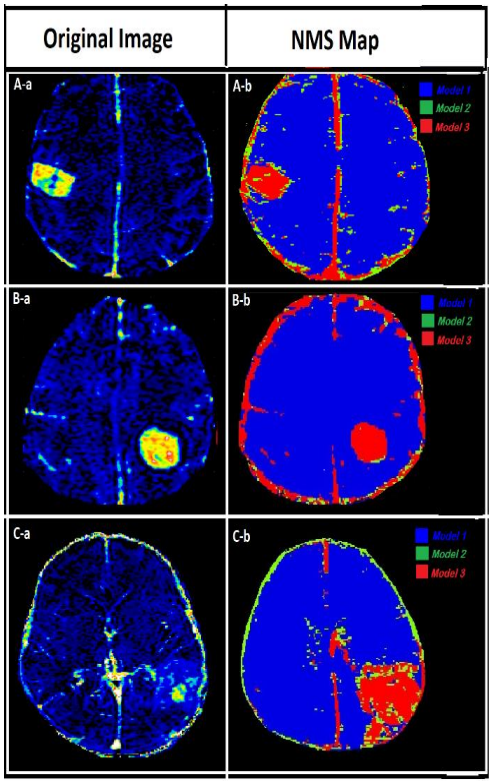

Figure 2. The first column illustrates the original brain image for three sample slices from three different patients and the second column shows their corresponding generated NMS maps

3.2. Deep-Net Segmentation Results

The Deep-Net was trained with a validation accuracy of 96.5% for segmentation of enhanced tumor, necrotic area, edema, and normal tissue and showed 88.7% performance ability for tumor region segmentation. In other words, there is an 11.3% chance of failure for the trained Deep-Net to provide a correct segment of the tumor, when it is applied to a new dataset. Thus, the trained Deep-Net has a generalizing error of ~0.11. The calculated Dice similarity coefficient of the employed Deep-Net on BraTS2020 dataset was obtained 0.77. Figure 3 illustrates the three examples of segmentation maps generated by Deep-Net for three sample slices.

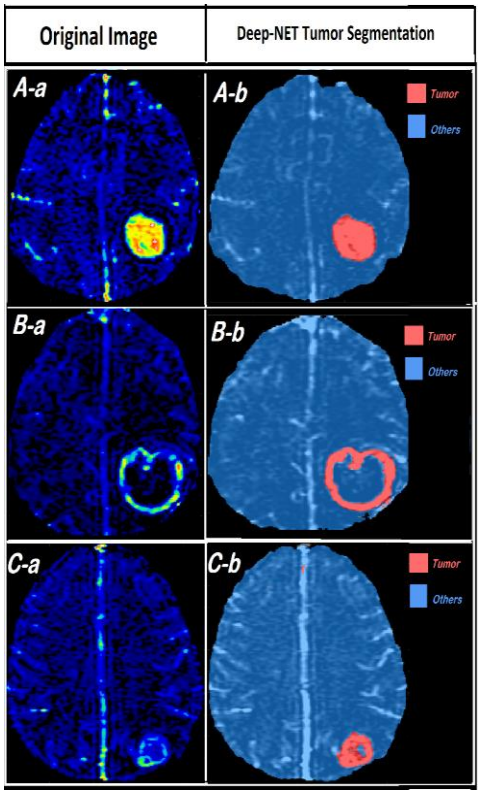

Figure 3. The first column implies the original brain image which was used as the test input of the deep CNN and the second column shows the predictive tumor region by red color over the brain image

The first column shows the original brain input images as the deep CNN and the second column shows the brain image with segmented enhanced tumor regions by Deep-Net overlay on it (red color). As observed in this figure, the enhanced tumor is accurately segmented from surrounding tissues such as edema, necrosis, and normal tissues. Since the used data is T1 contrast-enhanced MRI and the CA first fills the major vessels and then distribute across the other

brain tissue, thus the contrast concentration is high in the vessels especially in the large vessels. So in T1-wieghted images, the large vessels appear with an enhanced contrast intensity similar to the tumor region and this leads to false positive results in network decision. The results indicate that the Deep-Net may incorrectly assigns tumor label for some voxels located on the major vessels in a few slices, as shown in Figure 4. Notably, the enhanced voxels on the major vessels are correctly labeled as normal tissue in most tested slices, similar to sample slices in Figure 3. Figure 4 also implies that in a few slices the Deep-Net may fail to detect the tumor region, which is due to its generalization error (0.11).

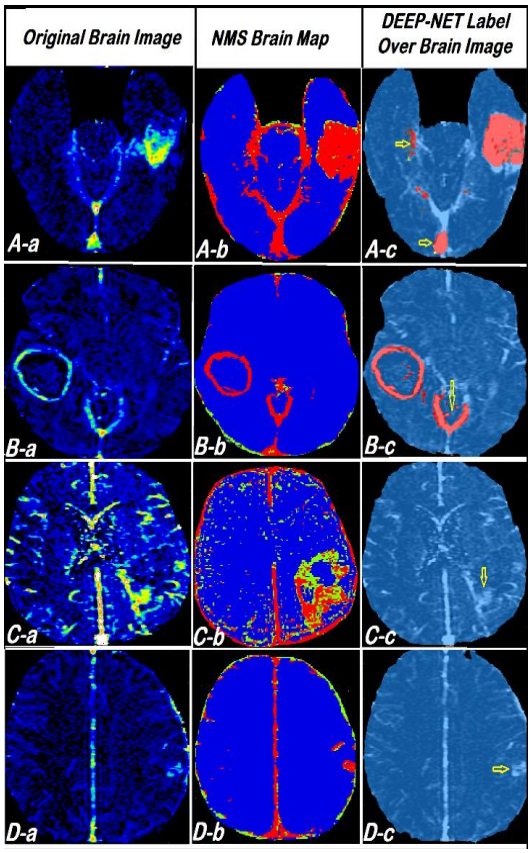

Figure 4. The first column implies the original brain image which was used as the test input of the deep CNN and the second column shows the generated NMS map for each slice, and the last column demonstrates the predictive tumor region by red color over the brain image

3.3. Comparison of the Results of the Two Segmentation Methods

Figure 5 compares the NMS tumor segmentation asa physiologic tumor segmentation with deep learning-based tumor segmentation for nine exemplary slices. As demonstrated in the figure, the first column is the original brain image, the second is the NMS map generated from pharmacokinetic analysis of DCE-MRI data, the third column is the predicted tumor region by the Deep-Net, the forth is the extracted tumor region from NMS map, the fifth is the extracted tumor region from Deep predicted map, the sixth is the overlay of two segmented tumor regions and the last column is the Dice (DSC), Jaccard (JSC) and Overlay (OLC) coefficients for the measurement of the overlapping information of two methods. As exhibited in this figure, the Deep-Net tumor segmentation is strongly in agreement with the tumor region delineated by the NMS technique. The obtained results imply that the trained Deep-Net and the NMS both reliably estimate the extent of the tumors for solid tumors (Figure 5-A,5-F, 5-H), ring- shaped tumors with necrotic core (Figure 5-B to 5-E and 5-L) or distributed tumors (Figure 5-G, 5-K). Figures 3 to 5 imply that according to the obtained similarity coefficients, the deep neural network used in this study can successfully adapt to the NMS segmented regions and distinguish the region and distribution of the tumor from the surrounding tissues in comparison with the NMS maps. However, in some cases, the Deep-Net has not been able to correctly detect the tumor, or in a few other slices, the voxels outside the tumor region especially the voxels on the large vessels are identified as tumors (see Figure 4). Furthermore, it is likely to misclassify the peritumoral regions as tumoral area through a wrong network decision (false positive). Most of these voxels on boundaries of the tumor are identified as Model 2 in the NMS technique, i.e. where the CA leaks to the interstitial space but is not allowed to return to the vasculature. Since, the Deep-Net classifies the regions based on the image intensity, it may incorrectly decide about these voxels as tumor region (false positive detection). It also seems that the boundaries of the tumor are more smoothed and uniformed in Deep-Net segmentation compared with the NMS technique. Also, in some cases a ring around the solid tumors is not detected as tumor region by the trained Deep-Net (false negative results), for example, see Figure 4 A-c. This issue may be due to generalization error and also the kind of the ground truth data (i.e. manual segmentation) used for training the Deep-Net, which was based on a region drawn by a group of radiologists.

The average similarity coefficient for each of the 25 patients was calculated and reported in Table 2. As can

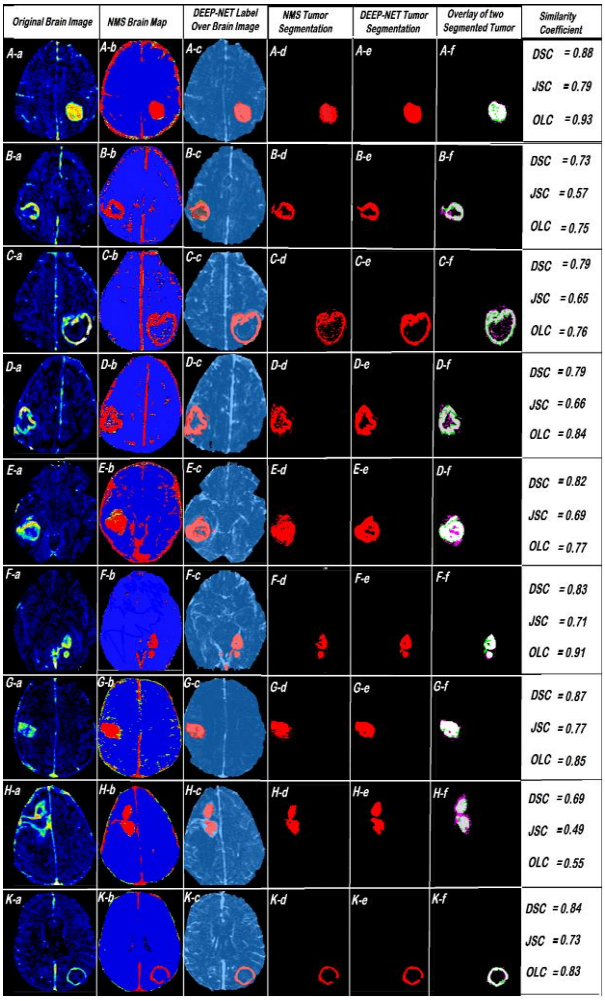

Figure 5. Comparison of the segmented tumor regions by NMS and Deep-Net techniques and measured similarity indexes (DSC, JSC, and OLC) for nine sample slices

be seen in this table, the similarity between two methods for a few patients is not very high, but the similarity coefficient is above the 80% for a few other patients. However, the averaged similarity coefficients over the all test data is above 66% for all three calculated scores (DSC: 0.73±0.15, JSC: 0.66±0.17, and OLC: 0.71±0.15). Relatively high similarity indexes indicate a close agreement between the two methods, and therefore show tumor segmentation capability of the applied Deep-Net.

4. Discussion

During the recent years, the concept of segmentation or distinguishing the tumor from the surrounding tissue has been regarded as one of the most critical and challenging issues in the field of image processing and analyzing. In this study, a Deep-Net based on the Deeplabv3+ and layers of resnet18 was trained using BraTS2020 dataset for segmentation of the tumor region in brain MR images. The acceptable Dice similarity coefficient was obtained for the Deep-Net segmentation and the manually segmented MR images, used as the ground truth for network training. The trained Deep-Net showed a high accuracy on the validation data for the segmentation of the enhanced tumor, necrotic area, edema, and normal tissue.

In the next step, the accuracy of this trained deep neural network in the segmentation of DCE-MRI images was compared with the NMS tumor segmentation, as a tissue pharmacokinetic-based segmentation.

Table 2. The average similarity coefficient calculated for each patient

Patient #	Dice Index (DSC)	Jaccard Index (JSC)	Overlay Index (OLC)
1	0.49	0.36	0.49
2	0.74	0.61	0.77
3	0.80	0.69	0.80
4	0.47	0.37	0.63
5	0.92	0.84	0.93
6	0.62	0.46	0.62
7	0.87	0.79	0.85
8	0.86	0.75	0.92
9	0.79	0.65	0.76
10	0.43	0.27	0.35
11	0.64	0.47	0.53
12	0.53	0.40	0.54
13	0.57	0.40	0.49
14	0.81	0.68	0.87
15	0.81	0.67	0.76
16	0.56	0.49	0.45
17	0.93	0.88	0.91
18	0.83	0.74	0.82
19	0.69	0.53	0.59
20	0.69	0.59	0.65
21	0.79	0.65	0.78
22	0.85	0.77	0.80
23	0.84	0.82	0.72
24	0.91	0.85	0.89
25	0.88	0.79	0.83
Averaged	0.73±0.15	0.66±0.17	0.71±0.15

The pharmacokinetic-based segmentation methods, compared with manual segmentation are less

dependent on human errors. A significant step in the pharmacokinetic analysis is the selection of the best model to fit the experimental data. According to the principle of parsimony, a model with fewer parameters has the best response if it describes the data behavior [34, 35]. Because of the presence of the noise in the data, the covariance effect of parameters on each other results in poor estimation for models with more describing parameters. So, it should be considered that the pharmacokinetic conditions of various pathologies are different and the best model with the least parameters should be selected to correctly estimate permeability parameters for each voxel [34, 35]. The nested model selection technique by assuming three different Models based on existing efflux and back flux of contrast agent between blood plasma and interstitial space can distinguish the different pathologies, and thus, NMS can be employed to physiologically segment the enhanced tumor region from its surrounding tissues. The NMS technique can be improved for other possible physiological conditions, such as necrotic areas in which there exists no contrast agent leakage into the extracellular extravascular space. For example, previous research [34] pointed out that Model 0 should be added to the NMS, describing the physiologic condition of necrotic tissues where the vasculature filing with CA is absent. As reported in the literature [16], the forward transfer constant in the peritumor edema is significantly higher than normal tissues. This property can be utilized to physiologically determine the edema boundaries in DCE-MRI data. Thence, it can be claimed that the use of the NMS technique with the DCE-MRI data for physiologic tumor segmentation is an efficient choice for providing the physiologic tumor labels as the gold standard in training a deep neural network for brain tumor segmentation. Of course, an unbiased and robust estimation method (such as utilized the MLE technique in this work [38]) is very necessary for relying on the NMS results [15, 43]. The results of this study and literature which used the NMS technique confirms that the tumor region can successfully be recognized in generated model selection maps in brain DCE-MRI studies [1, 34-37, 44, 45]. The findings of this pilot study confirm that the segmented tumor region by Deep-Net as a fast segmentation method is in close agreement with the determined tumor region in the NMS method, although the training process was performed using manually segmented images as the ground truth. Thus, the trained networks such as Deep-Net in this study can be reliably used in segmentation software, especially if its training process is completely independent of human expertise.

The supervised deep neural networks, which are usually used for image segmentation, are trained using images labeled by expert physiologists as ground truth. Manual segmentation of the tumor is a labor-based procedure and highly dependent on the expertise and experience of clinical radiologists and their slice-by-slice decisions about the tumor margins. Therefore, the training accuracy of such methods may be dependent on human expertise although this method provides the advantage of determination of different tumor regions, like necrotic tissue, enhancing tumor, non-enhancing tumor, and edema. The accuracy of the deep learning-based method used in this study can be significantly improved if the network is trained by the NMS segmentation approach, which is completely automatic, without dependency on human experience, and decision.

One of the main advantages of deep CNN segmentation over other methods is its fast, and automatic feature extraction due to its convolution layers [18]. This substantial advantage reduces the dependency of this method to image pre-processing procedures, which are sometimes performed manually or by applying approximations [18], thus the effect of human error on the result will be minimized.

5. Conclusion

The utilized deep learning approach in this work has been shown relatively accurate and reliable segmentation to be employed in clinical application. Using machine learning in clinical practice may facilitate and speed up the segmentation process, in addition to accurate, precise, and automate segmentation. Therefore, if an artificial neural network such as Deep-Net is supposed to be used in clinical software, it would be better to train it via a set of the data and ground truth labels that are completely independent of any human errors. Since training the neural networks with the manual methods as ground truth is a little dependent on the radiologists determining the tumor regions, it may cause a dependency on the human expertise and accuracy. Besides, the training process needs to be performed just once and then the trained network can be used for fast

clinical experiment analysis. Thus, it is proposed that a deep neural network is first trained by a set of DCE-MRI data, and then the trained network is used more confidently in clinical practice for other imaging modalities such as T1 contrast-enhanced (T1-ce) or Fluid-attenuated inversion recovery (FLAIR) MR imaging. Utilization of the DCE-MRI sequence and employing the NMS segmentation approach as the gold standard in the training process make a fully automated training process for the network which is completely independent of human errors.

References

1- A. N. V. Dehkordi, A. Kamali-Asl, N. Wen, T. Mikkelsen, I. J. Chetty, and H. Bagher-Ebadian, "DCE-MRI prediction of survival time for patients with glioblastoma multiforme: using an adaptive neuro-fuzzy-based model and nested model selection technique," (in eng), *NMR in biomedicine*, vol. 30, no. 9, Sep 2017, doi: 10.1002/nbm.3739.

2- S. A. Naji, R. Zainuddin, and H. A. Jalab, "Skin segmentation based on multi pixel color clustering models," *Digital Signal Processing*, vol. 22, no. 6, pp. 933-940, 2012/12/01/ 2012, doi: https://doi.org/10.1016/j.dsp.2012.05.004.

3- S. Saravanan, R. Karthigaivel, and V. Magudeeswaran, "A brain tumor image segmentation technique in image processing using ICA-LDA algorithm with ARHE model," *Journal of Ambient Intelligence and Humanized Computing*, 2020/03/29 2020, doi: 10.1007/s12652-020-01875-6.

4- M. Agn *et al.*, "A modality-adaptive method for segmenting brain tumors and organs-at-risk in radiation therapy planning," *Medical Image Analysis*, vol. 54, pp. 220-237, 2019/05/01/ 2019, doi: https://doi.org/10.1016/j.media.2019.03.005.

5- B. Leena and A. Jayanthi, "Brain tumor segmentation and classification via adaptive CLFAHE with hybrid classification," *International Journal of Imaging Systems and Technology*, vol. 30, no. 4, pp. 874-898, 2020, doi: https://doi.org/10.1002/ima.22420.

6- A.Rajendran and R. Dhanasekaran, "Fuzzy Clustering and Deformable Model for Tumor Segmentation on MRI Brain Image: A Combined Approach," *Procedia Engineering*, vol. 30, pp. 327-333, 2012/01/01/ 2012, doi: https://doi.org/10.1016/j.proeng.2012.01.868.

7- A. Bhandari, J. Koppen, and M. Agzarian, "Convolutional neural networks for brain tumour segmentation," *Insights into Imaging*, vol. 11, no. 1, p. 77, 2020/06/08 2020, doi: 10.1186/s13244-020-00869-4.

8- Y. Wang, C. Li, T. Zhu, and C. Yu, "A Deep Learning Algorithm for Fully Automatic Brain Tumor Segmentation," in *2019 International Joint Conference on Neural Networks (IJCNN)*, 2019: IEEE, pp. 1-5.

9- G. Wang, W. Li, S. Ourselin, and T. Vercauteren, "Automatic Brain Tumor Segmentation Based on Cascaded Convolutional Neural Networks With Uncertainty Estimation," (in English), *Frontiers in Computational Neuroscience*, Original Research vol. 13, no. 56, 2019-August-13 2019, doi: 10.3389/fncom.2019.00056.

10- M. H. Hesamian, W. Jia, X. He, and P. Kennedy, "Deep Learning Techniques for Medical Image Segmentation: Achievements and Challenges," *Journal of Digital Imaging*, journal article vol. 32, no. 4, pp. 582-596, August 01 2019, doi: 10.1007/s10278-019-00227-x.

11- M. Havaei *et al.*, "Brain tumor segmentation with Deep Neural Networks," *Medical Image Analysis*, vol. 35, pp. 18-31, 2017/01/01/ 2017, doi: https://doi.org/10.1016/j.media.2016.05.004.

12- A. Işın, C. Direkoğlu, and M. Şah, "Review of MRI-based Brain Tumor Image Segmentation Using Deep Learning Methods," *Procedia Computer Science*, vol. 102, pp. 317-324, 2016/01/01/ 2016, doi: https://doi.org/10.1016/j.procs.2016.09.407.

13- H. Dong, G. Yang, F. Liu, Y. Mo, and Y. Guo, "Automatic brain tumor detection and segmentation using U-Net based fully convolutional networks," in *annual conference on medical image understanding and analysis*, 2017: Springer, pp. 506-517.

14- F. Isensee and K. Maier-Hein, "An Attempt at Beating the 3D U-Net. 2019," *arXiv preprint arXiv:1908.02182*.

15- A. N. Dehkordi and S. Koohestani, "The Influence of Signal to Noise Ratio on the Pharmacokinetic Analysis in DCE-MRI Studies," *Frontiers in Biomedical Technologies*, 2019.

16- M. Zhao *et al.*, "Quantitative analysis of permeability for glioma grading using dynamic contrast-enhanced magnetic resonance imaging," (in eng), *Oncol Lett*, vol. 14, no. 5, pp. 5418-5426, 2017, doi: 10.3892/ol.2017.6895.

17- S. Bakas, H. Akbari, and A. Sotiras, "Segmentation labels for the pre-operative scans of the TCGA-GBM collection. The Cancer Imaging Archive," ed, 2017.

18- R. Yamashita, M. Nishio, R. K. G. Do, and K. Togashi, "Convolutional neural networks: an overview and application in radiology," *Insights into Imaging*, vol. 9, no. 4, pp. 611-629, 2018/08/01 2018, doi: 10.1007/s13244-018-0639-9.

19- C. Wachinger, M. Reuter, and T. Klein, "DeepNAT: Deep convolutional neural network for segmenting

neuroanatomy," (in eng), *NeuroImage*, vol. 170, pp. 434-445, 2018, doi: 10.1016/j.neuroimage.2017.02.035.

20- J. Amin, M. Sharif, M. Raza, and M. Yasmin, "Detection of Brain Tumor based on Features Fusion and Machine Learning," *Journal of Ambient Intelligence and Humanized Computing*, 2018/11/01 2018, doi: 10.1007/s12652-018-1092-9.

21- X. Kong, G. Sun, Q. Wu, J. Liu, and F. Lin, "Hybrid pyramid u-net model for brain tumor segmentation," in *International conference on intelligent information processing*, 2018: Springer, pp. 346-355.

22- M. Lopez and J. Ventura, "Dilated Convolutions for Brain Tumor Segmentation in MRI Scans," in *BrainLes@MICCAI*, 2017.

23- F. Chollet, "Xception: Deep Learning with Depthwise Separable Convolutions," in *2017 IEEE Conference on Computer Vision and Pattern Recognition (CVPR)*, 21-26 July 2017 2017, pp. 1800-1807, doi: 10.1109/CVPR.2017.195.

24- M. Marcinkiewicz, J. Nalepa, P. R. Lorenzo, W. Dudzik, and G. Mrukwa, "Segmenting brain tumors from MRI using cascaded multi-modal U-Nets," in *International MICCAI Brainlesion Workshop*, 2018: Springer, pp. 13-24.

25- M. Rezaei, H. Yang, K. Harmuth, and C. Meinel, "Conditional generative adversarial refinement networks for unbalanced medical image semantic segmentation," in *2019 IEEE Winter Conference on Applications of Computer Vision (WACV)*, 2019: IEEE, pp. 1836-1845.

26- R. Pourreza, Y. Zhuge, H. Ning, and R. Miller, "Brain tumor segmentation in mri scans using deeply-supervised neural networks," in *International MICCAI Brainlesion Workshop*, 2017: Springer, pp. 320-331.

27- G. Kim, "Brain tumor segmentation using deep fully convolutional neural networks," in *International MICCAI Brainlesion Workshop*, 2017: Springer, pp. 344-357.

28- K. Pawar, Z. Chen, N. J. Shah, and G. Egan, "Residual encoder and convolutional decoder neural network for glioma segmentation," in *International MICCAI Brainlesion Workshop*, 2017: Springer, pp. 263-273.

29- R. Thillaikkarasi and S. Saravanan, "An enhancement of deep learning algorithm for brain tumor segmentation using kernel based CNN with M-SVM," *Journal of medical systems*, vol. 43, no. 4, p. 84, 2019.

30- M. W. Nadeem *et al.*, "Brain tumor analysis empowered with deep learning: A review, taxonomy, and future challenges," *Brain Sciences*, vol. 10, no. 2, p. 118, 2020.

31- R. A. Zeineldin, M. E. Karar, J. Coburger, C. R. Wirtz, and O. Burgert, "DeepSeg: deep neural network framework for automatic brain tumor segmentation using magnetic resonance FLAIR images," *International Journal of Computer Assisted Radiology and Surgery*, vol. 15, no. 6, pp. 909-920, 2020/06/01 2020, doi: 10.1007/s11548-020-02186-z.

32- K. Kamnitsas *et al.*, "Efficient multi-scale 3D CNN with fully connected CRF for accurate brain lesion segmentation," *Medical image analysis*, vol. 36, pp. 61-78, 2017.

33- P. S. Tofts *et al.*, "Estimating kinetic parameters from dynamic contrast-enhanced t1-weighted MRI of a diffusable tracer: Standardized quantities and symbols," *Journal of Magnetic Resonance Imaging*, vol. 10, no. 3, pp. 223-232, 1999, doi: 10.1002/(sici)1522-2586(199909)10:3<223: aid-jmri2>3.0.co;2-s.

34- H. Bagher-Ebadian *et al.*, "Model Selection for DCE-T1 Studies in Glioblastoma," *Magn Reson Med*, vol. 68, no. 1, pp. 241-251, 2012, doi: 10.1002/mrm.23211.

35- J. R. Ewing, R. Elmghirbi, and T. Nagaraja, "Chapter 20 - Dynamic Contrast-Enhanced Magnetic Resonance Imaging in Brain Tumors," in *Nervous System Drug Delivery*, R. R. Lonser, M. Sarntinoranont, and K. Bankiewicz Eds.: Academic Press, 2019, pp. 405-428.

36- J. R. Ewing *et al.*, "Model selection in magnetic resonance imaging measurements of vascular permeability: Gadomer in a 9L model of rat cerebral tumor.," *J Cereb Blood Flow Metab*, vol. 26, no. 3, pp. 310-320, 2006

37- D. A. N.V., K. A. Alireza, E. J. R., W. Ning, C. I. J., and B. E. Hassan, "An adaptive model for rapid and direct estimation of extravascular extracellular space in dynamic contrast enhanced MRI studies," *NMR in biomedicine*, vol. 30, no. 5, p. e3682, 2017, doi: doi:10.1002/nbm.3682.

38- H. Bagher-Ebadian, A. Dehkordi, and J. Ewing, "SU-F-I-26: Maximum Likelihood and Nested Model Selection Techniques for Pharmacokinetic Analysis of Dynamic Contrast Enhanced MRI in Patients with Glioblastoma Tumors," *Medical Physics*, vol. 43, no. 6, pp. 3392-3392, 2016, doi: doi:http://dx.doi.org/10.1118/1.4955854.

39- L. R. Dice, "Measures of the Amount of Ecologic Association Between Species," *Ecology*, vol. 26, no. 3, pp. 297-302, 1945, doi: https://doi.org/10.2307/1932409.

40- T. J. Sørensen, *A method of establishing groups of equal amplitude in plant sociology based on similarity of species content and its application to analyses of the vegetation on Danish commons*. København: I kommission hos E. Munksgaard (in English), 1948.

41- P. Jaccard, "THE DISTRIBUTION OF THE FLORA IN THE ALPINE ZONE.1," *New Phytologist*, vol. 11, no. 2, pp. 37-50, 1912, doi: https://doi.org/10.1111/j.1469-8137.1912.tb05611.x.

42- M. Vijaymeena and K. Kavitha, "A survey on similarity measures in text mining," *Machine Learning and Applications: An International Journal*, vol. 3, no. 2, pp. 19-28, 2016.

43- A. N. Dehkordi, "The Effect of the Bias in the Contrast Agent Concentration Measurement on the Estimated Pharmacokinetic Parameters in Brain Dynamic Contrast Enhanced Magnetic Resonance Imaging Studies," *Iranian Journal of Medical Physics*, pp. -, 2019, doi: 10.22038/ijmp.2019.41400.1598.

44- A. N. V. Dehkordi *et al.*, "Dynamic Contrast Enhanced MR Estimation of Pharmacokinetic Parameters of Glioblastoma Multiforme Tumors: A Comparison Study for Peritumoral and Global Arterial Input Functions Using Model Selection Technique," *Neuro-Oncology*, vol. 17, no. 5, pp. 165-166, November 1, 2015 2015, doi: 10.1093/neuonc/nov225.52.

45- J. R. Ewing and H. Bagher-Ebadian, "Model selection in measures of vascular parameters using dynamic contrast-enhanced MRI: experimental and clinical applications," (in eng), *NMR in biomedicine*, vol. 26, no. 8, pp. 1028-1041, 2013, doi: 10.1002/nbm.2996.